Journal of Hydrology 576 (2019) 85–97

Contents lists available at ScienceDirect

Journal of Hydrology

journal homepage: www.elsevier.com/locate/jhydrol

Research papers

Data-driven stochastic model for basin and sub-grid variability of SMAP satellite soil moisture

Navid Jadidoleslam[a,*], Ricardo Mantilla[a], Witold F. Krajewski[a], Michael H. Cosh[b]

[a] IIHR-Hydroscience & Engineering, The University of Iowa, Iowa City, IA 52242, USA
[b] USDA-ARS Hydrology and Remote Sensing Laboratory, Beltsville, MD 20705-2350, USA

ARTICLE INFO

This manuscript was handled by Marco Borga, Editor-in-Chief

Keywords:
Soil moisture
Variability
Satellite
Remote sensing
Sub-grid
Basin

ABSTRACT

This study focused on the utility of coarse surface soil moisture observations for applications that require high resolution surface soil moisture information. This was accomplished by quantifying the information content of average soil moisture for three different spatial scales of 81 km^2, 790 km^2, and 4400 km^2. In situ point observations of soil moisture from 31 stations in Iowa were used to develop a spatial stochastic model that assumes hillslope-scale model parameters are independent. Soil moisture dry-downs and wetting regimes were analyzed using rain gauge and soil moisture sensor data. The statistical nature of dry-downs were parameterized using a power-law decay, and soil moisture increases due to rainfall were parameterized using a non-dimensional logistic curve that is a function of soil moisture deficit. The resulting stochastic model is used to quantify the magnitude of the standard deviation, $\sigma(\theta)$, and skewness $G(\theta)$ as a function of the areal average. We show that the greatest information content (small spatial standard deviation) of average observation corresponded to values near the minimum or the maximum soil moisture with $\sigma(\theta) < 5\%$, while average observations for intermediate soil moisture values had the lowest information content with $\sigma(\theta) > 20\%$. The differences in information content as a function of the areal average were consistent with the statistical nature of soil moisture that can be interpreted as small range bounded variable. However, this study provides quantitative estimates for the magnitude of the sub-grid and basin scale variability, documenting the utility for applications that require high resolution information. These results form the basis for the investigation of spatial runoff production in response to rainfall and to inform plot scale agriculture applications.

1. Introduction

Surface soil moisture is a key state variable linking short-term and long-term water and energy balances in the soil and the atmosphere (Yang et al., 2016) and land-atmosphere interactions (Entekhabi et al., 1996) that determine evaporation and evapotranspiration (Koster et al., 2004), and surface runoff production leading to extreme flooding (Grillakis et al., 2016). It also plays a major role in plant ecology, environmental biology (Orchard and Cook, 1983), and carbon cycle through plant respiration (Boone et al., 1998).

The most common technique for field-scale soil moisture measurement is using soil TDR (Time Domain Reflectometry) probes (Topp et al., 1980; Romano, 2014). However, due to high spatial variability of soil moisture in space (Western et al., 2004; Yang et al., 2017), using this measurement technique is neither feasible nor practical for larger spatial scales. Therefore, remote sensing techniques are being employed as a more efficient alternative to track soil moisture in space and time. NASA SMAP (Soil Moisture Active Passive) is the most recent satellite mission to focus on global soil moisture observations (Entekhabi et al., 2010) launched in 2015 that uses L-band (1.4 GHz) radiometer.

Satellite soil moisture estimations have coarse spatial resolution (e.g. Enhanced SMAP L3 ~9 km) due to limitations in large antenna size needed for L-band microwave measurements (Njoku and Entekhabi, 1996; Kerr, 2007). Therefore, understanding information content of the satellite soil moisture and its spatial variability for sub-grid and basin scales is essential for its hydrologic applications.

Several studies focused on characterization of the measured soil moisture distribution and its spatial variability over time using field observations (e.g. Famiglietti et al. (1997), Ryu and Famiglietti (1997), Choi and Jacobs (2007), Brocca et al. (2012), Cho and Choi (2014)). Rosenbaum et al. (2012) used 150 sensor observations to study soil moisture spatial variability and showed that groundwater influenced locations have higher spatial variability than other locations. Famiglietti et al. (2008) analyzed the soil moisture spatial variability at

* Corresponding author.
E-mail address: navid-jadidoleslam@uiowa.edu (N. Jadidoleslam).

https://doi.org/10.1016/j.jhydrol.2019.06.026
Received 11 September 2018; Received in revised form 4 June 2019; Accepted 9 June 2019

spatial scales ranging from 800 (m) to 50 (km). Their analysis demonstrated that larger spatial extents have higher variability. Brocca et al. (2014) compared variability of absolute soil moisture, degree of saturation and soil moisture anomalies with respect to long-term mean for 6 observation networks with areas ranging from 250 to 150,000 km^2.

In addition to studies based on observations only, there have been studies that used modeling approach to investigate soil moisture variability. For example, Teuling and Troch (2005) used a soil moisture balance model to estimate soil moisture variability in 3 different sites. Controls of soil hydraulic properties, specifically van Genuchten-Mualem parameters, on the relationship between soil moisture spatial variability with its mean has been investigated by different studies (e.g. García et al. (2014), Qu et al. (2015), Wang et al. (2015)). Zarlenga et al. (2018) adopted a stochastic model of unsaturated flow to investigate the effects of a scaling triplet (spacing, extent and support introduced by Andrew and Günter (1999)) on the soil moisture spatial variability.

Chaney et al. (2015) used the TOPLATS model (Sivapalan et al., 1987) to estimate watershed scale spatial variability of root-zone soil moisture using fine scale (~500 m) radar rainfall data. Application of three dimensional hydrologic model for estimation of soil moisture variability has also been investigated by Cornelissen et al. (2014) and Gebler et al. (2017). Reported results from those two modeling studies indicate underestimation of spatial variability from modeled soil moisture compared to observations. For details on current status of soil moisture spatio-temporal variability research, the reader is referred to Section 3 of Brocca et al. (2017) and Section 8 in Babaeian et al. (2018).

In previous studies, soil moisture sensor observations play a key role in understanding spatial and temporal variability of soil moisture and evaluation of soil moisture estimations from model simulations. These studies demonstrate the added value of field measurements of soil moisture. The main objective of this study is to investigate soil moisture variability within SMAP satellite sub-grid and basin spatial scales by analyzing soil moisture sensor and rain gauge observations and using higher resolution radar rainfall and soil properties to approximate spatial statistics of surface soil moisture.

Section 2 describes the domains of study and data characteristics that are used. Section 2.3, discusses the methodology for extraction of the soil dry-downs and wetting phases, the parameterization of each phase, and a description of the soil moisture model. In Results and Discussion (Section 3), we compare stochastic model results with SMAP and soil moisture sensor(s) for one SMAP pixel within each basin and at the basin scale. Thereafter, we investigate the soil moisture spatial statistics of the proposed model and compare it with field observations and SMAP satellite soil moisture.

2. Materials and methods

2.1. Study area

Two watersheds (Fig. 1) located in Iowa are the focus of this study. Iowa is located in a warm and humid continental climate zone (e.g. Peel et al. (2007)) with an annual average precipitation of 870 mm (1981–2010). The Turkey River basin is located at northeast Iowa and has a drainage area of 4400 km^2. It is approximately 56% cropland, 14% pasture, 13% of the basin is forested, and the remaining area is grassland and developed. The South Fork basin is located in north-central Iowa with a drainage area of 790 km^2. Cropland dominates the land cover with 88% of the total area. The main soil texture, based on USDA classes, for the Turkey River and South Fork basins are silt-loam and loam, respectively.

2.2. Data

2.2.1. Field measurements

Fig. 1 shows available soil moisture and rain gauges in the state of Iowa, USA. At each site, 4 soil moisture sensors are installed at depths of 5, 10, 20 and 50 cm. This study will focus on the 5 cm depth of soil column at each site. The IFC (Iowa Flood Center) TDR probes are Campbell CS655 (Campbell Scientific Inc., 2012) and the USDA-ARS soil moisture sensors are Stevens Hydra probes (Stevens, 2018). Both soil moisture sensors have a reported accuracy from ± 1 to ± 3% volumetric soil moisture. At each site, dual tipping bucket rain gauges are collocated with the soil moisture sensors. It has been shown that dual tipping bucket rain gauges for rainfall measurements increases the measurement reliability (Ciach et al., 1999).

The temporal coverage of the soil moisture and rainfall data for different sites is shown in Fig. 2. For quality control of soil moisture data, we followed Dorigo et al. (2011) for detection of errors in soil moisture time series. We applied a manual quality control on the soil moisture sensor data. We removed the cold season time periods (November 1–March 31), highlighted as gray in Fig. 2, to avoid possible erroneous soil moisture readings due to frozen top soil layer. Also, we used rainfall data from two tipping bucket rain gauges at each site to check the soil moisture time series. If there was rainfall more than 5 mm and soil moisture did not increase during a 24-h period, we avoided using the data. We did not remove temperature-related diurnal fluctuations in soil moisture because these fluctuations are within the specified accuracy of sensors.

2.2.2. Radar rainfall & satellite soil moisture

For rainfall, we used MRMS (Multi Radar Multi Sensor), a rain gauge bias-corrected radar rainfall product (Zhang et al., 2016) that has approximately a 1-km resolution. We employed hourly rainfall from April to November 2016 as forcing for estimation of the soil moisture for each hillslope which is discussed in the Section 2.3.3.

Enhanced Level 3 Version 1 (hereafter L3) SMAP (Chaubell et al., 2016) soil moisture product has approximately 9 km resolution with global revisit time of 2–3 days. SMAP soil moisture estimations are provided by NASA on EASE-Grid 2 (hereafter SMAP grid). There are 21 and 73 SMAP pixels that intersect with South Fork and Turkey River basins, respectively. We use SMAP soil moisture for comparisons with sensor observations and simulated hillslope soil moisture.

2.2.3. Soil properties

Two soil properties used in this study are porosity and residual soil moisture. These two values, for 0–5 cm soil layer, were obtained from the POLARIS soil properties database, which is a probabilistic soil series map for the contiguous United States and has a 30 (m) spatial resolution (Chaney et al., 2016).

2.3. Methods

Field-scale soil moisture dynamics could be classified into two phases. Soil moisture dry-down that is due to drainage and evaporation/evapotranspiration while soil wetting is due to rainfall and/or irrigation, noting that most of the agricultural fields in Iowa are rain-fed.

We analyzed the soil moisture dry-downs and wetting phases of soil moisture time series. Then, we parameterized these two phases and used the distributions of parameters for estimation of the hillslope surface soil moisture forced with MRMS rainfall.

2.3.1. Dry-down periods

The dry-down time periods of surface soil moisture were identified using local minimum and maximums of the soil moisture time series. A threshold peak prominence value of 0.02 (m^3/m^3) was used and the dry-down curves that last at least 12 h were selected. Also, dry-downs with more than 2 mm accumulated rainfall were excluded from the analysis.

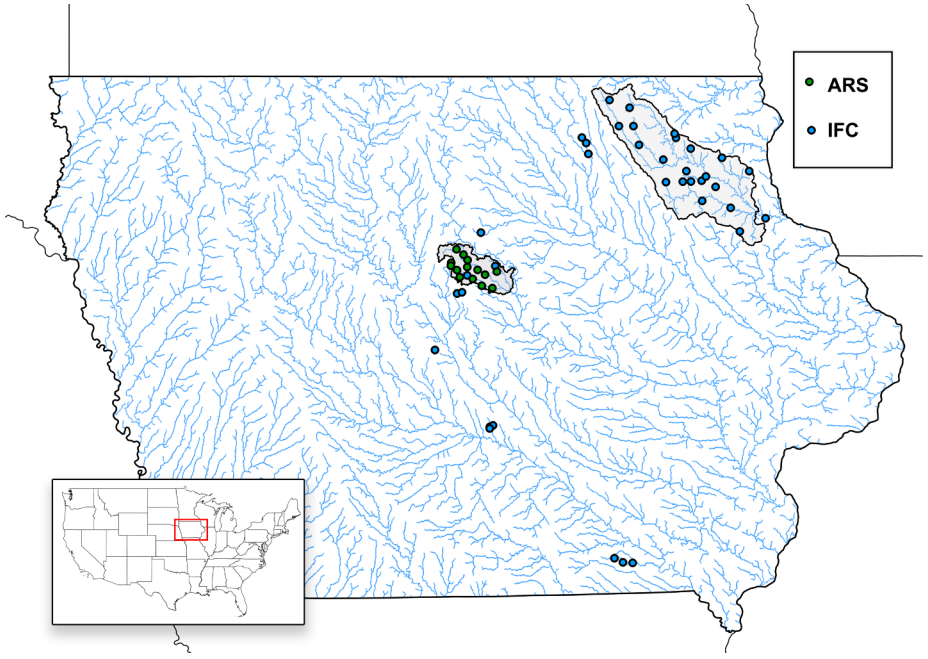

Fig. 1. Locations of the stations used in this study for IFC (Iowa Flood Center) and ARS (Agricultural Research Service) stations shown in blue and green, respectively. (For interpretation of the references to colour in this figure legend, the reader is referred to the web version of this article.)

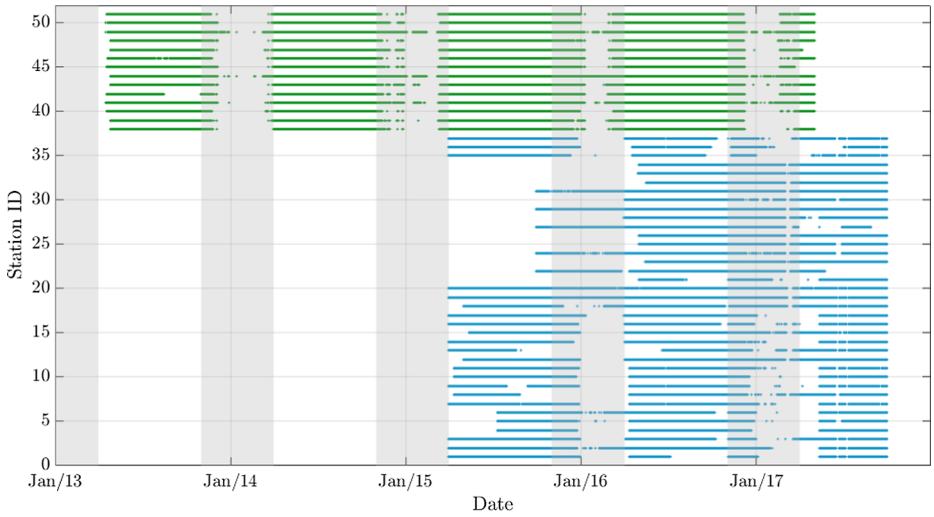

Fig. 2. Temporal coverage for ARS (green) and IFC (blue) soil moisture-rain gauges used in this study. Shaded gray color indicate the time periods that are excluded from the analysis. (For interpretation of the references to colour in this figure legend, the reader is referred to the web version of this article.)

Consequently, 2352 dry-down events are employed in the study.

Rondinelli et al. (2015) and Shellito et al. (2016) used an exponential equation with different mathematical forms for fitting the soil moisture dry-down curves using 3 parameters. For this study, we selected a power-law model with two parameters for fitting the dry-down curves, to improve flexibility and to decrease the number of parameters required,

$$SM_{t-\tau} = (SM_{\tau} - SM_r)[(\beta - 1)(\alpha(t-\tau) + 1)]^{\frac{1}{1-\beta}} + SM_r \quad (1)$$

where SM_{τ} is soil moisture at the initiation of dry-down, $SM_{t-\tau}$ is soil moisture at any time $t - \tau$ elapsed from the dry-down initiation and SM_r is residual soil moisture, which is assumed as minimum soil moisture of the time series.

Eq. (1) is fitted to extracted dry-down curves from soil moisture observations with a non-linear least square method to find α and β for each dry-down curve. Fig. 4 shows the normalized dry-down curves based on initial soil moisture of the dry-downs for IFC soil moisture sensors with elapsed time ($t - \tau$) in days. Each of the fitted curves have different dry-down parameters (α, β). Fitted and observed dry-down curves have a good agreement with an RMSE (root mean square error) and coefficient of determination of 0.006 cm^3/cm^3 and 0.95, respectively.

2.3.2. Wetting phase

The total rainfall and magnitude of soil moisture increase during rainfall events are found for each wetting time periods from soil moisture time series. An example of these periods are highlighted as blue in Fig. 3. Using a similar approach described in Section 2.3.1 with an inter-event dry period of 2 h, we found positive soil moisture change and total rainfall depth. We detected 4334 wetting periods across the sensor histories.

Hardie et al. (2013) investigated soil moisture change with respect to rainfall for 0–90 (cm) depths. They were able to find “weak but

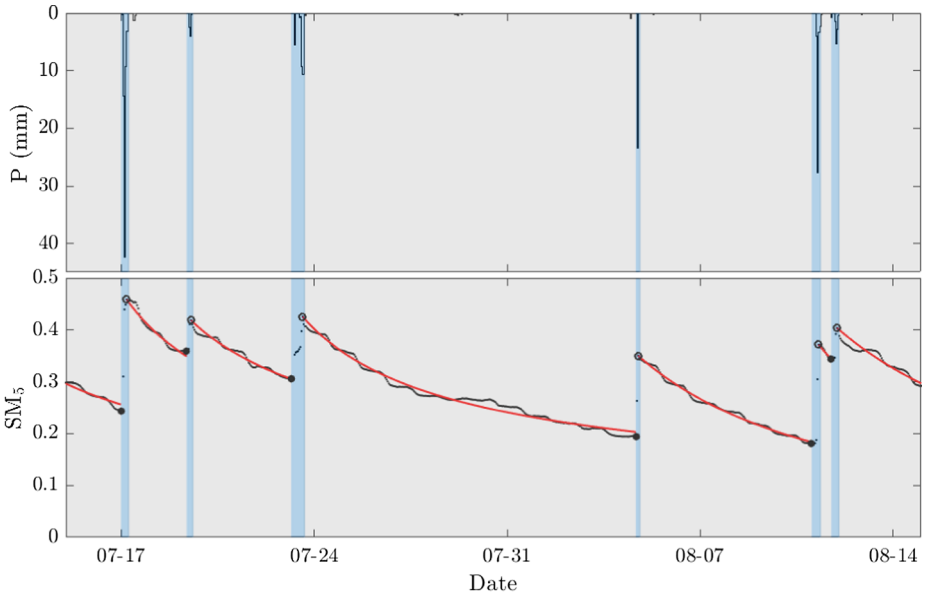

Fig. 3. Example rainfall and soil moisture observations (black) for wetting (blue), drying periods (gray) and dry-down fitted curves (red). Black dots and circles correspond to soil moisture before and after rainfall event. (For interpretation of the references to colour in this figure legend, the reader is referred to the web version of this article.)

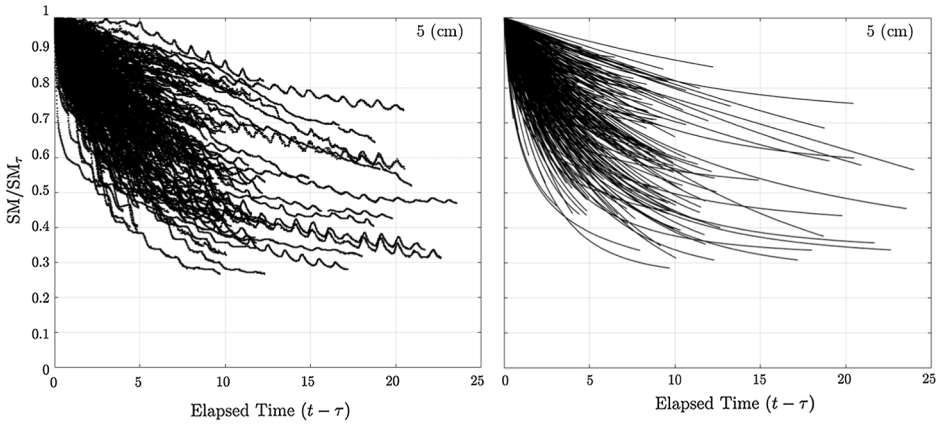

Fig. 4. Measured (left) and fitted (right) soil dry-down curves for IFC soil moisture sensors at 5 cm depth.

significant relationship between the amount of precipitation and soil moisture change". In our study, we only used surface soil moisture measurements (5 cm depth) and we normalized the magnitude of soil moisture increase, over the wetting period, by soil moisture deficit ($\phi - SM_i$), defined as the difference between soil porosity and initial soil moisture before initiation of the rainfall event. Furthermore, we normalized total rainfall by the sensing depth of soil moisture sensor and soil moisture deficit.

Fig. 5 shows the non-dimensional deficit-normalized soil moisture increase with respect to deficit-normalized rainfall over wetting periods for all of the stations in this study. Each point demonstrates what percentage of available space at top layer soil is filled up by rainfall. Most of the data points are close to one-to-one line while soil moisture change is higher for higher magnitudes of deficit-normalized rainfall. In the case of an ideal bucket model, one may expect that deficit-normalized soil moisture increase of surface soil layer should correspond with deficit-normalized rainfall magnitudes. In other words,

$$\frac{SM_f - SM_i}{\phi - SM_i} = \begin{cases} \frac{\sum P}{(\phi - SM_i)d_{sv}} & \text{if} \frac{\sum P}{(\phi - SM_i)d_{sv}} < 1 \\ 1 & \text{if} \frac{\sum P}{(\phi - SM_i)d_{sv}} \geqslant 1. \end{cases}$$

Our data analysis shows that there is uncertainty in soil moisture change with respect to rainfall. There are different factors that could be contributing to the scattering of the data points in Fig. 5. Changes in soil porosity, macropores and preferential flow (e.g. Beven and Germann (1982)) could contribute to the scattering. Preferential flow can also contribute to larger deficit-normalized soil moisture increase than deficit-normalized rainfall magnitude, which is neglected in our study due to insignificant instances of these events.

Investigating the effect of above-mentioned factors on soil moisture change has its own challenges (Guo et al., 2018) and does not fit in the scope of this study given the limitations of the available information and temporal resolution of rainfall and soil moisture observations. Nevertheless, it is important to account for these factors in hydrologic modeling and the authors would like to express the need for further research.

An asymptotic equation (Eq. (2)) with one parameter (γ) is chosen to solve for each point shown in Fig. 5,

$$SM_f = SM_i + \frac{\frac{\sum P}{d_{sv}}}{\left[1 + \left(\frac{\sum P}{d_{sv}(\phi - SM_i)}\right)^{\gamma}\right]^{1/\gamma}} \quad (2)$$

where $\sum P$ is the total rainfall depth over the wetting period, ϕ is soil porosity assumed as maximum soil moisture of the observations at each station, d_{sv} is effective depth of sensing volume for the soil moisture sensors used in this study, which is approximately 75 mm. SM_i and SM_f are soil moisture before and after the soil moisture wetting event, also shown as black circles and black dots in Fig. 3, respectively. Solving Eq.

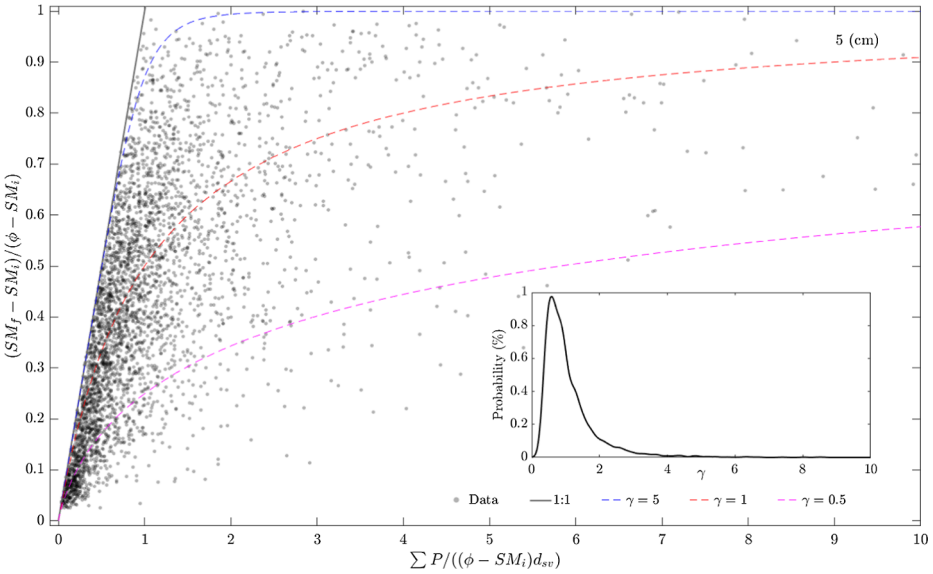

Fig. 5. Deficit-normalized soil moisture increase and deficit-normalized rainfall for wetting periods across all soil moisture sensors for 5-cm depth. Examples of the fits with 3 different γ values are shown with dashed line. Right corner: Distribution of the fitted soil moisture wetting parameter (γ).

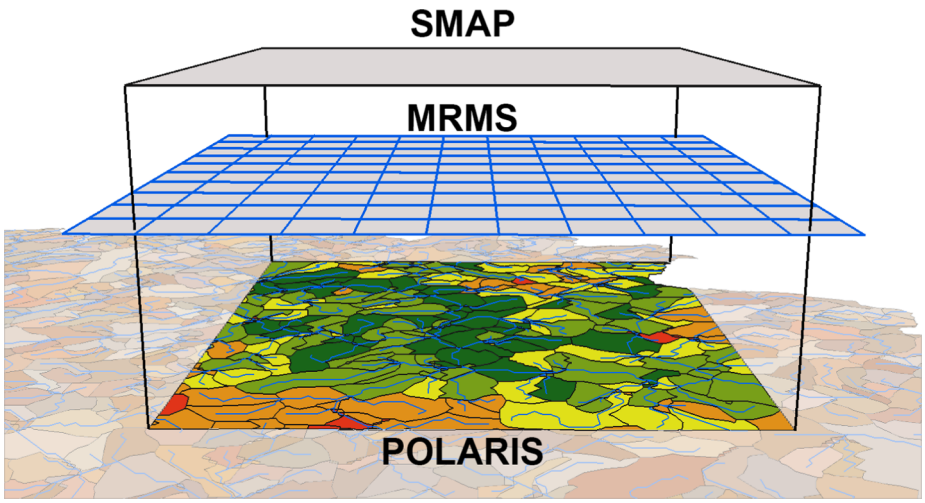

Fig. 6. SMAP pixel (9 km × 9 km), MRMS grid (1 km × 1 km) and corresponding hillslopes within one SMAP grid with median area of 0.3 km^2.

(2) for each point in Fig. 5 gives different γ values for which its distribution is shown in Fig. 5. We note that, the functional form in Eq. (2) imposes a constraint on the soil moisture increase to be less than or equal to its deficit.

We investigated a possible relationship between the dry-down curve parameters (α and β) and geophysical attributes of each site including soil temperature, soil texture, slope. We could not find any clear and distinct relationship between soil moisture dry-down parameters (α, β) and these attributes. However, we found similarity in normalized dry-down rates but also significant variability in normalized soil moisture (SM/SM_τ) dry-downs for concurrent dry-downs across stations.

2.3.3. Numerical modeling

A surface soil moisture time series was generated based on Eq. (1) and Eq. (2). We note that, the fitted dry-down parameters are discrete in time because we only have one pair of α and β for a single dry-down curve. Therefore, to have sufficient number of parameter samples and to account for variability of dry-down parameters in different time of year, a soil moisture dry-down is generated, right after cessation of rainfall, as follows: First, we select the dry-down parameters that are within a 40-day time window ($\tau \pm 20$ days) of dry-down initiation time (or rainfall cessation time), denoted as τ in Eq. (1). Then, we construct non-parametric distributions, from which we sample α and β. Finally, by plugging sampled parameters into Eq. (1), we estimate the soil moisture dry-down until the next rainfall initiation time.

Note that as it is shown in Eq. (1), a soil moisture dry-down only depends on the initial soil moisture of the dry-down (SM_τ) which is calculated from a previous wetting, residual soil moisture (SM_r) from POLARIS database, and α and β which are randomly sampled for each dry-down as described above.

For soil moisture wetting, during a rainfall event, we randomized the soil moisture response to each pulse of rainfall. First, we sample from the distribution of wetting phase parameter (γ) shown in Fig. 5. Then, we calculate the soil moisture change by plugging the sampled γ into Eq. (2) while the initial soil moisture SM_i is already calculated either from the final value of a dry-down or soil moisture of the previous time step of a wetting. We repeat this procedure until rainfall ends. We use hourly MRMS rainfall at each hillslope by calculating the area-weighted average rainfall of the contributing MRMS pixels.

The initial soil moisture of the hillslopes on April 1st 2016 were generated randomly with a uniform distribution ranging from residual saturation to soil porosity.

Simulations are conducted for each basin separately with their corresponding calculated parameters. We note that, Turkey River and South Fork basins have approximately 10,800 and 1800 hillslopes, respectively. Fig. 6 shows a schematic of one SMAP pixel, intersecting MRMS rainfall grid and hillslopes. Each SMAP grid consists of approximately 100 MRMS grids and more than 300 hillslopes.

Normalized soil moisture standard deviation and skewness are compared with its mean for model and sensor observations. Also, these three statistics are calculated for SMAP soil moisture and upscaled model soil moisture over Turkey River basin. For upscaling the model soil moisture to SMAP pixel resolution, spatial mean of normalized model soil moisture is calculated for hillslopes that are within SMAP pixel. Thereafter, upscaled model soil moisture time series is subset, over time, by using the matching timestamps of SMAP satellite overpass.

The differences in spatial variability of absolute soil moisture and normalized soil moisture (degree of saturation) is shown by Brocca et al. (2014). Hence, for spatial statistics (mean, standard deviation and skewness) of sensor observations, model and SMAP soil moisture, we used normalized soil moisture or effective saturation, defined as

$$\theta = \frac{SM - SM_r}{\phi - SM_r} \tag{3}$$

where θ is normalized soil moisture (degree of saturation) that changes from 0 to 1, SM is volumetric water content that can change between residual soil moisture (SM_r) and soil porosity (ϕ). For sensor observations, we used minimum and maximum soil moisture of the sensor history as porosity and residual soil moisture, respectively. For normalization of model soil moisture and SMAP soil moisture, we used POLARIS soil porosity and residual soil moisture.

For the sake of completeness, definitions of mean, standard deviation and skewness are given in Eqs. (4)–(6).

$$E[\theta] = \frac{1}{N}\sum_{i=1}^{N} \theta_i \tag{4}$$

$$\sigma[\theta] = \sqrt{\sum_{i=1}^{N} (\theta_i - E[\theta])} \tag{5}$$

$$G[\theta] = \frac{1}{N}\frac{\sum_{i=1}^{N} (\theta_i - E[\theta])^3}{(\sigma[\theta])^3} \tag{6}$$

where N is the number of hillslopes, θ_i is normalized soil moisture at i-th hillslope and $E[\theta]$ is the mean soil moisture of the hillslopes.

It is important to highlight that the independence of point scale model parameters does not imply independence of the time series that are generated. A strong correlation between sites is maintained because spatial patterns of precipitation are correlated.

3. Results and discussions

3.1. SMAP sub-grid soil moisture

Soil moisture estimates for one SMAP pixel inside Turkey River and South Fork basins are shown in Figs. 7 and 8, respectively. We selected SMAP pixels that contain at least one soil moisture sensor which are highlighted with red color in these figures. Longitude and latitude of the centroid for SMAP pixel in Turkey River basin and South Fork are −91.4680, 42.7813 and −93.4537, 42.4914 (decimal degrees), respectively. The top panel shows hourly MRMS rainfall averaged over hillslopes within one SMAP pixel. The color scale shows the soil moisture probability of occurrence ($p(SM)$) inside the SMAP grid for April-November 2016. Descending and ascending swaths of the SMAP satellite are shown with downward and upward triangles. Also, time series of soil moisture sensor(s) collocated with SMAP pixel is shown in black line.

For SMAP pixels within each basin, soil moisture from SMAP and in situ stations were inside the range of modeled soil moisture. Higher rainfall magnitudes tended to increase the probability of higher soil moisture within SMAP pixel from model. Overall, SMAP soil moisture wettings and dry-downs agreed with the model and sensor. However, generally SMAP soil moisture estimations are lower than other two. More specifically, SMAP soil moisture is drier than sensor and model soil moisture from June to September.

3.2. Basin-scale soil moisture

Figs. 9 and 10, from top to bottom panel, show basin-averaged hourly rainfall from the MRMS product, simulated soil moisture probability of occurrence over time with median soil moisture of all of the hillslopes within each basin (red line), the corresponding SMAP soil moisture as box plots with dark and light gray colors, referring to AM and PM swaths of SMAP satellite and time series of soil moisture observations inside each basin. The maximum number of sensors used for Turkey River basin and South Fork are 15 and 16, respectively.

There was good agreement between sensor observations and simulated time series of soil moisture where sensor observations are within the range of simulated soil moisture for the two basins. In few cases, specifically for South Fork, sensor observations exceeded the saturation level of the model that could be originating from either flow accumulation at soil moisture sensor location or lower soil porosity used in the model.

SMAP soil moisture observations lie inside the simulated range. However, there are moments in time where SMAP estimations are lower than residual saturation. More specifically, SMAP soil moisture for South Fork basin exhibited lower soil moisture values than the residual saturation for June-August 2016. This could be due to the vegetation growing season in Iowa, where L-band radiometric sensitivity to vegetation water content (VWC) increases that conversely decreases sensitivity to soil moisture (Neelam and Mohanty, 2015). Spatial variability of SMAP soil moisture for South Fork was less than Turkey River due to the smaller watershed area and thus fewer SMAP pixels.

SMAP soil moisture estimates tend to dry-down faster than estimated soil moisture of the hillslopes which is consistent with the study on the SMAP moisture dry-down rates (Shellito et al., 2016) and an overall assessment of SMAP soil moisture products (Chan et al., 2016). Chen et al. (2018) speculated that underestimation in auxiliary surface temperature of SMAP could be one of the contributors to dry-bias of SMAP soil moisture estimates.

3.3. Standard deviation and skewness

Hourly standard deviation with respect to mean of normalized model and observed soil moisture for Turkey River and South Fork are shown in Fig. 11. Standard deviation is maximum in the intermediate range of soil moisture, while it is lower for low and high soil moisture mean values. The overall trend and dynamic range for the mean and standard deviation of observed soil moisture is captured by the model.

For Turkey River basin, the standard deviation of the modeled and observed soil moisture for wet conditions was lower than dry conditions, while for South Fork basin, the lower limits of standard deviation for wet and dry conditions had similar values. For the time period of our study, maximum standard deviation of observed soil moisture for Turkey River basin (Fig. 11a) is 0.29 cm^3/cm^3 with mean value of 0.54 cm^3/cm^3 whereas the peak standard deviation of observations for South Fork (Fig. 11b) is approximately 0.30 cm^3/cm^3 at mean soil moisture of 0.35 cm^3/cm^3.

Soil moisture variability results by Gebler et al. (2017) using hydrologic model were lower than the observed soil moisture spatial variability because of uniform atmospheric forcing (e.g. rainfall) and vegetation over their study domain. Modeled soil moisture variability

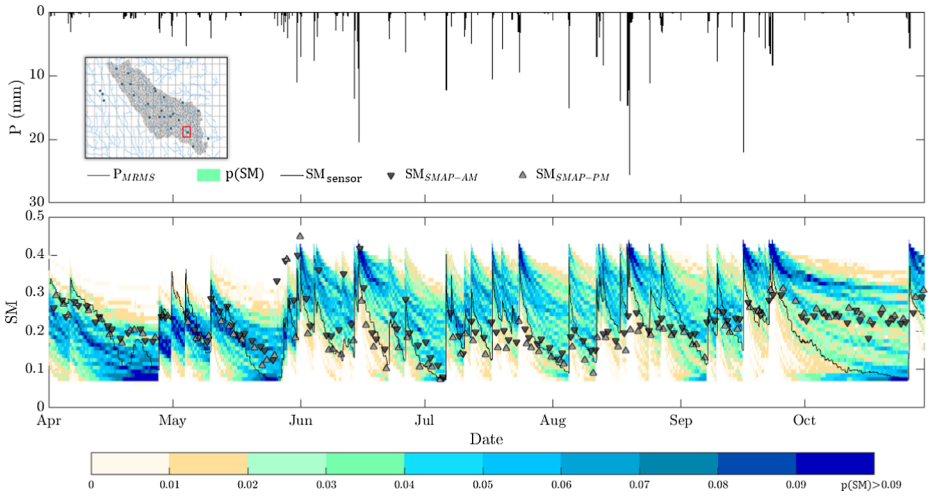

Fig. 7. Sub-grid soil moisture probability time series for a SMAP pixel within Turkey River basin from April to November 2016. Top panel: Location of SMAP pixel (highlighted red) and sub-grid area-averaged rainfall time series; Bottom panel: Enhanced L3 SMAP (AM: downward triangle, PM: upward triangle) and sensor soil moisture (black) overlayed with simulated probabilistic soil moisture for hillslopes within SMAP pixel. (For interpretation of the references to colour in this figure legend, the reader is referred to the web version of this article.)

results from Cornelissen et al. (2014) also showed an underestimation compared to observations due to homogeneous rainfall forcing. In contrast to these two studies, our model results for soil moisture variability are slightly higher than observations which can be attributed to rainfall variability in space.

Fig. 12 shows changes of skewness with mean soil moisture for Turkey River and South Fork basins, respectively. Soil moisture skewness of the model and observations show good agreement for both watersheds. The distribution is negatively skewed for wet conditions while skewness becomes positive for dry conditions. This result is in the same line with conclusions by Famiglietti et al. (2008).

While general patterns of standard deviation and skewness with respect to mean are captured by the proposed model, there are differences in modeled and observed normalized soil moisture statistics with respect to its mean. One reason for this difference could be due to normalization of observations by using maximum and minimum of the soil moisture sensor history as porosity and residual soil moisture.

Note that, the number of hillslopes (sample size) for which the statistics are calculated in Figs. 11 and 12 is not same as the number of sensor observations in these basins. Therefore, for comparisons between observed and modeled soil moisture standard deviation and skewness, same number of hillslopes as the number of sensor observations was selected, randomly, inside each basin and statistics were calculated for each group. Accordingly, Figs. 13 and 14 correspond to standard deviation and skewness of normalized soil moisture with respect to its mean. These two figures show the statistics for groups of 15 and 16 hillslopes for Turkey River and South Fork basins. Dynamic range of the statistics in these two figures, cover the standard deviation and skewness of the soil moisture sensor observations within each basin. In contrast to South Fork basin, modeled soil moisture standard deviations reach zero for very wet conditions in Turkey River basin because of high rainfall spatial extent. The range of observed soil moisture skewness for Turkey River basin and South Fork are within the range of ensemble skewness of the model. Turkey River basin is 6 times larger than South Fork, therefore the range for soil moisture standard deviation and skewness is higher for a given mean. Previous studies such as Andrew and Günter (1999) and Famiglietti et al. (2008) have shown that as spatial extent increases, soil moisture standard deviation increases.

Our results show that normalized soil moisture standard deviation is maximum at intermediate range ($\theta \sim 0.5$). These results are consistent with the findings from previous studies (e.g. Famiglietti et al. (1998), Choi and Jacobs (2007), Famiglietti et al. (2008), Rosenbaum et al. (2012), Cho and Choi (2014)), where the relationship between standard deviation of soil moisture with its mean was found to be downward concave (upward convex). We note that, upper bound of variance for a bounded random variable follows Bhatia-Davis inequality (Bhatia and Davis, 2000),

$$\sigma^2[\theta] \leqslant (M - E[\theta])(E[\theta] - m) \tag{7}$$

where θ is normalized soil moisture that is bounded between M = 1 and m = 0. The maximum possible variance is 0.25 that corresponds to $E[\theta] = 0.5$, while variance is zero at the two bounds. Therefore, the upward convex relationship between mean and standard deviation/

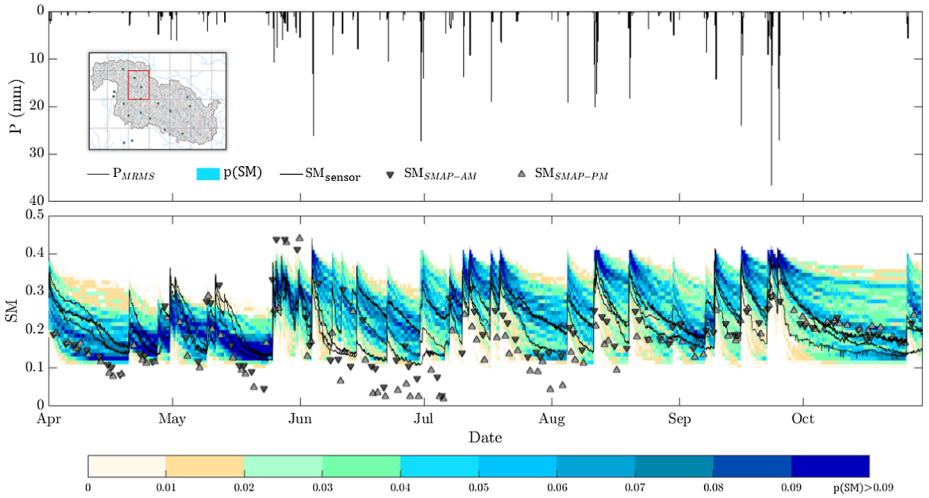

Fig. 8. Sub-grid soil moisture probability time series for a SMAP pixel within South Fork basin from April to November 2016. Top panel: Location of SMAP pixel (highlighted red) and sub-grid area-averaged rainfall; Bottom panel: Enhanced L3 SMAP (AM: downward triangle, PM: upward triangle) and three sensor soil moisture overlayed with simulated probabilistic soil moisture for hillslopes within SMAP pixel.

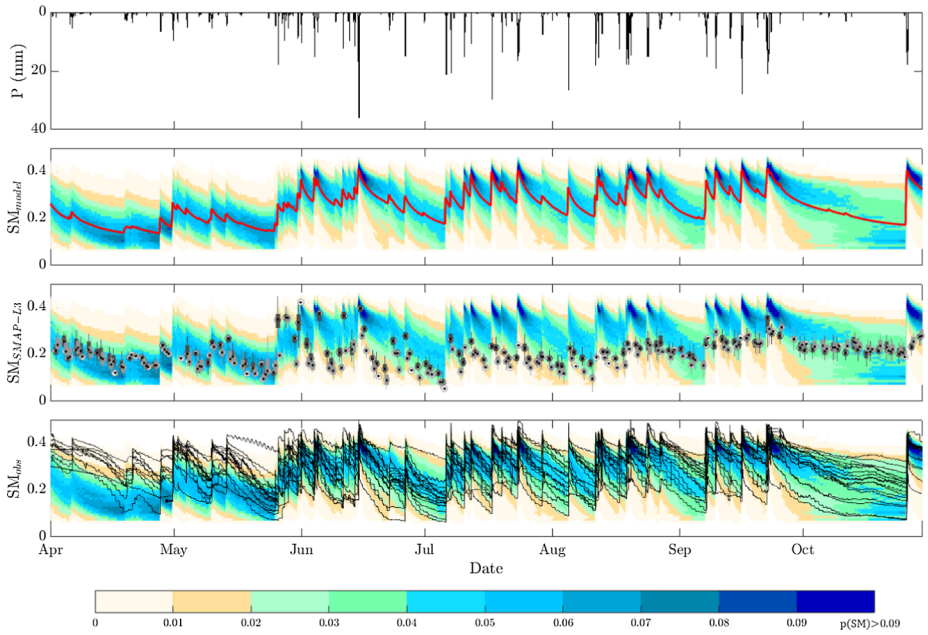

Fig. 9. Probabilistic soil moisture time series for Turkey River basin for year 2016. From top to bottom: basin-averaged hourly rainfall, probability of simulated 5-cm soil moisture and median soil moisture (red line), Enhanced L3 SMAP soil moisture boxplots (AM: dark gray, PM: light gray) and soil moisture time series of sensors inside this basin. (For interpretation of the references to colour in this figure legend, the reader is referred to the web version of this article.)

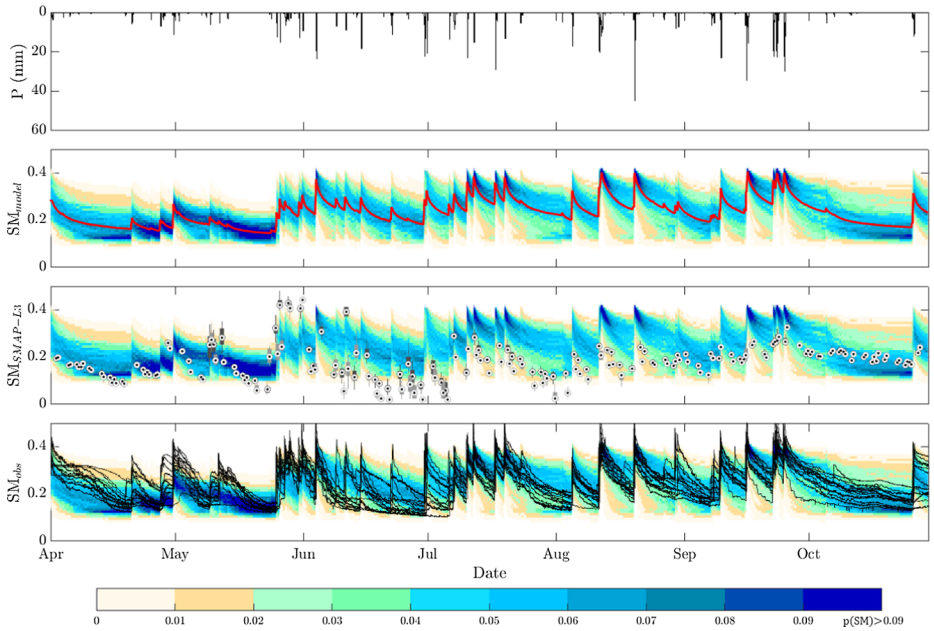

Fig. 10. Probabilistic soil moisture time series for South Fork basin for year 2016. From top to bottom: basin-averaged hourly rainfall, probability of simulated 5-cm soil moisture and median soil moisture (red line), Enhanced L3 SMAP soil moisture boxplots (AM: dark gray, PM: light gray) and soil moisture time series of sensors inside this basin. (For interpretation of the references to colour in this figure legend, the reader is referred to the web version of this article.)

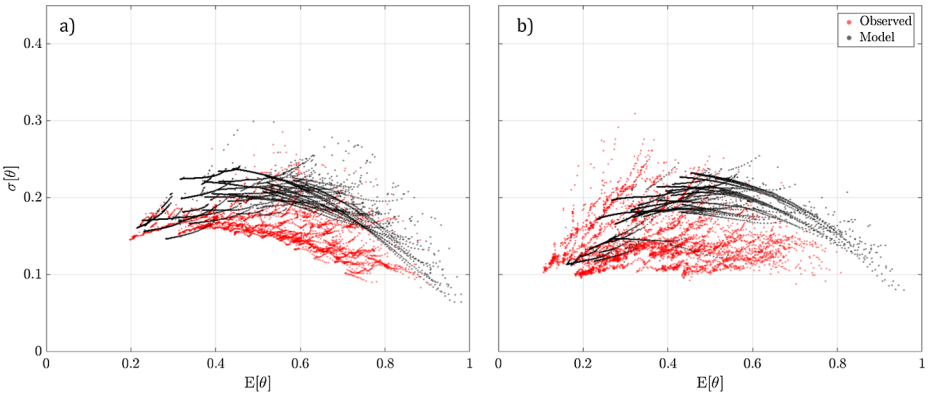

Fig. 11. Hourly soil moisture standard deviation with respect to its mean for observed (red) and simulated (black) soil moisture for (a) Turkey River basin and (b) South Fork basin. (For interpretation of the references to colour in this figure legend, the reader is referred to the web version of this article.)

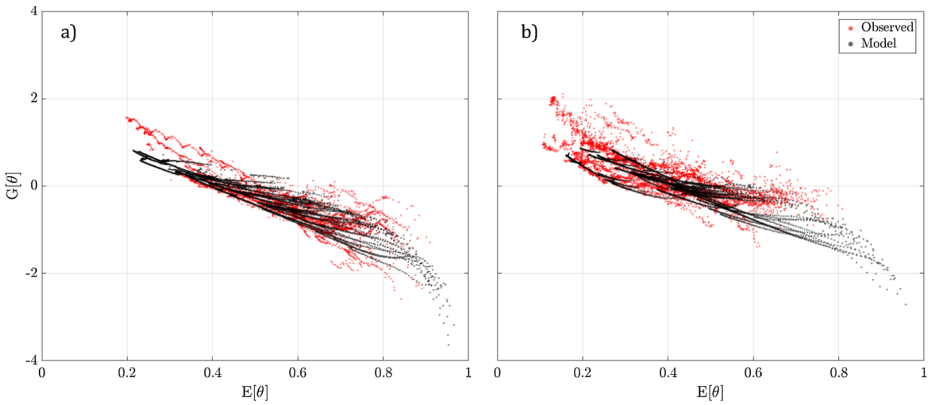

Fig. 12. Hourly soil moisture skewness with respect to its mean for the observed (red) and simulated (black) soil moisture for (a) Turkey River basin and (b) South Fork basin. (For interpretation of the references to colour in this figure legend, the reader is referred to the web version of this article.)

variance of normalized soil moisture is its inherent statistical property.

We further compare the variations of normalized soil moisture statistics over time using the same approach described previously for generating results shown in Figs. 13 and 14. Fig. 15 shows model approximations for upper and lower bounds of soil moisture standard deviation and skewness over time for Turkey River and South Fork basins.

Soil moisture variability and skewness decreases for rainfall events with high spatial extent. Temporal variations of standard deviation and skewness for observations and model generally have good agreement.

As previously shown in Fig. 10, the observed sensor soil moisture values are within the range of modeled soil moisture over time, while, there are few instances in time where standard deviation of the observations is slightly lower than that of approximated possible standard deviations for South Fork basin (Fig. 15c). Note that, as it is discussed by Chaney et al. (2015), lack of soil moisture sensors in wet regions will lead to underestimation in standard deviation compared to model estimations, specially over dry periods.

3.4. Spatial variability and skewness of SMAP soil moisture

Spatial statistics of upscaled model and SMAP satellite soil moisture over Turkey River basin are also calculated. Fig. 16 shows standard deviation and skewness of SMAP soil moisture and upscaled model soil moisture over Turkey River basin for 65 pixels whereas each pixel covers at least 20 hillslopes. Upward and downward triangles in this figure correspond to ascending (PM) and descending (AM) SMAP satellite orbits, respectively. The standard deviation and skewness of upscaled model soil moisture and SMAP satellite soil moisture over Turkey River basin are in a similar dynamic ranges. However, the mean values of SMAP satellite soil moisture are generally lower than mean of upscaled model soil moisture. Compared to spatial variability of soil moisture in basin scale, which is shown in Fig. 11a, Fig. 16a suggests that standard deviation of upscaled model is lower due to averaging of hillslope soil moisture over SMAP pixels that has approximate support length of 9 km. This result is consistent with findings from Andrew and Günter (1999) and Zarlenga et al. (2018) that showed increasing support length decreases soil moisture spatial variance. Fig. 16b shows skewness for upscaled model and SMAP soil moisture over Turkey River basin. There is similar trend as shown in Fig. 12a whereas skewness is negative for wet and becomes positive in dry conditions for SMAP and upscaled model.

As previously mentioned, we averaged the soil moisture of the hillslopes collocated with a given SMAP pixel. Although averaging as an upscaling approach shows comparable results in terms of soil moisture variability, however as Njoku and Entekhabi (1996) suggested, due to horizontal heterogeneities within satellite footprint, the retrieved "average" soil moisture of satellite remote sensing, in most of the cases may not be representative of the spatial average of soil moisture. Further studies on this aspect using data from field campaigns such as SMAPVEX campaigns can help in understanding the spatial aggregation scheme of the satellite.

4. Summary & conclusions

In this study, we focused on the parameterization of dry-down and wetting phases of surface soil moisture and extraction of the parameter distributions for each phase using 31 rainfall and soil moisture measurements over two basins. We used the extracted statistical information from soil moisture sensors and we simulated surface soil moisture at each hillslope by bringing higher resolution information on soil properties and rainfall. We compared observed, modeled and SMAP

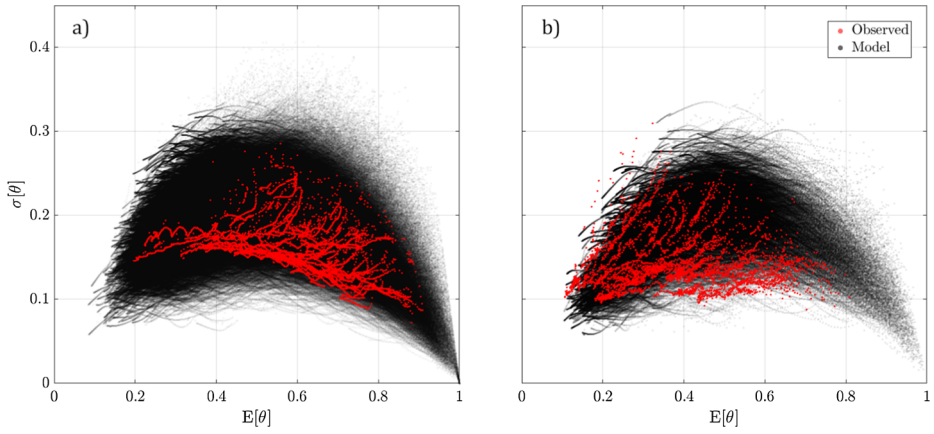

Fig. 13. Normalized soil moisture standard deviation with respect to its mean for observation sensors (red) and simulated soil moisture for groups of hillslopes (black) for (a) Turkey River basin (b) South Fork basin. (For interpretation of the references to colour in this figure legend, the reader is referred to the web version of this article.)

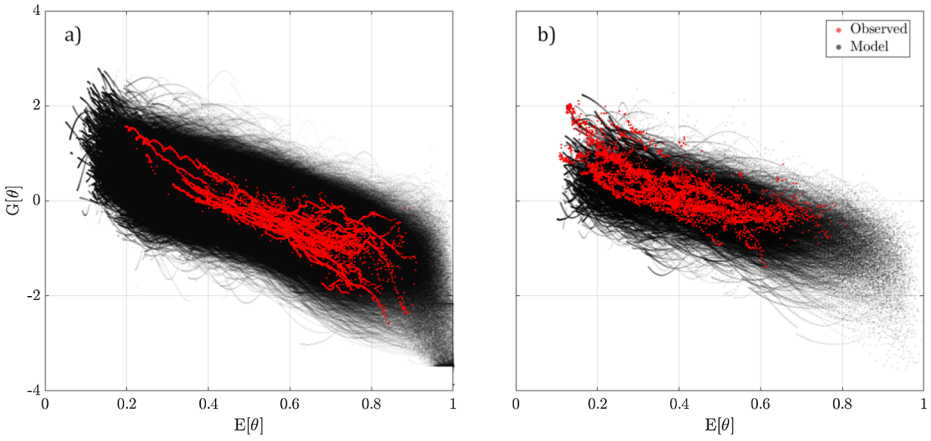

Fig. 14. Normalized soil moisture skewness with respect to its mean for observation sensors (red) and simulated soil moisture for groups of hillslopes (black) in (a) Turkey River basin (b) South Fork basin. (For interpretation of the references to colour in this figure legend, the reader is referred to the web version of this article.)

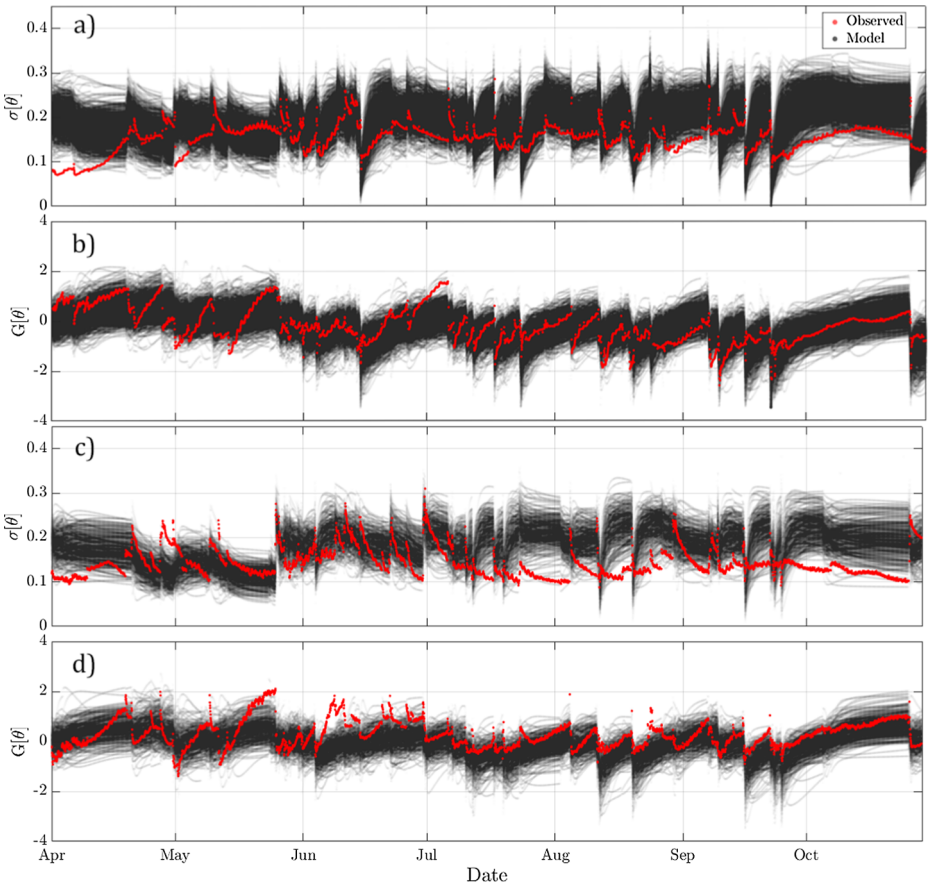

Fig. 15. Temporal variations of normalized soil moisture standard deviation ($\sigma[\theta]$) and skewness ($G[\theta]$) with respect to its mean for 15 and 16 observation sensors (red) and simulated soil moisture for groups of 15 and 16 hillslopes (black) for Turkey River (a & b) and South Fork (c & d) basins. (For interpretation of the references to colour in this figure legend, the reader is referred to the web version of this article.)

satellite soil moisture estimates over the study period. Furthermore, we investigated sub-grid and basin-scale soil moisture variability. Taking all the above-mentioned points into consideration, the following conclusions can be drawn:

- SMAP soil moisture responded to rainfall events while generally it increased less than observed and modeled soil moisture for the study period. In most of the cases, SMAP underestimated soil moisture during dry-down periods. There were only few cases where SMAP soil moisture was slightly higher than observed and modeled soil moisture.
- Satellite soil moisture retrievals are sensitive to VWC (vegetation water content). SMAP uses a 10-year (2000–2010) climatological average for VWC which is derived from MODIS (Kim, 2013). SMAP estimates for Turkey River basin were slightly higher than South Fork. Part of this could be due to less cropland proportion in Turkey River basin (56%) compared to South Fork (88%).
- Field observations of soil moisture for the two basins corresponded very well with the modeled soil moisture where they lie inside the range of simulated soil moisture for 2016. Moreover, standard

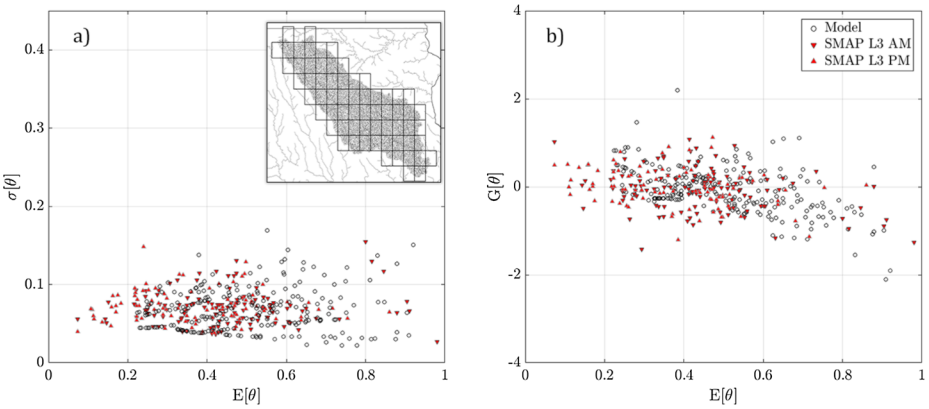

Fig. 16. (a) Standard deviation and (b) skewness of the upscaled model and SMAP soil moisture over Turkey river basin for 65 SMAP pixels. Upward and downward triangles correspond to AM and PM swaths of SMAP satellite, respectively.

deviation and skewness of the two watersheds exhibited different behaviors from each other, originating from different soil properties and wetness, which was captured by the proposed model, thus demonstrating the model skill in replicating the soil moisture statistics.

- In theory, for two extreme cases of very wet and dry conditions with large spatial extent over the basins, the distribution of soil moisture for a given basin should approach to distributions of soil porosity and residual soil moisture over the study area.
- Our results indicate that for dry, wet and medium soil moisture conditions, soil moisture skewness become positive, negative and close to zero, respectively, which is consistent with findings from previous studies (e.g. Cho and Choi (2014), Famiglietti et al. (1997)).
- We show that as the number of hillslopes/samples, for which the statistics are calculated, increases, for a given mean soil moisture, uncertainty in standard deviation and skewness decreases.
- Spatial variability and skewness of the upscaled model soil moisture is found to be comparable with SMAP soil moisture over Turkey River basin suggesting that averaging over larger support length decreases variability.

The relationship between soil moisture variability with its mean from soil moisture sensors and the proposed model implies that uncertainty in soil moisture for two cases of wet and dry conditions decreases to values close to zero. This relationship could be used as an insight for inferring the information content of the satellite soil moisture estimations and its applications.

We have compared our results with satellite soil moisture in terms of spatial variability in basin scale and in probabilistic sense for sub-grid scale. Further research is needed for connecting the information content of satellite estimations to field-scale or hillslope-scale soil moisture while analysis of data from field campaigns could be helpful with this respect.

In this study, we only addressed the surface soil moisture dynamics which is more relevant to satellite soil moisture. Our methodology could be used in basins that have soil moisture observations, such as international soil moisture networks (Dorigo et al., 2011), and ground-based radar rainfall (Zhang et al., 2016; Harrison et al., 2009) or satellite rainfall products (e.g. Huffman et al. (2015)) for estimating basin-scale or satellite soil moisture sub-grid variability.

The main limitation of our study is that its application depends on availability of recent historical soil moisture sensor, rain gauge data for analysis and fine resolution radar rainfall data for simulations.

Future studies developed by this methodology could account for longer time periods, the errors in radar rainfall and uncertainty in soil properties for more accurate depiction of basin and sub-grid soil moisture distributions. Also, our study demonstrated the importance of field observations for further understanding of the surface soil moisture variability. This methodology could be expanded to lower soil layers, by extracting statistical information from soil moisture observations at each depth and coupling between them, for partitioning of rainfall to runoff and more specifically, drought and flood forecasting.

CRediT authorship contribution statement

Navid Jadidoleslam: Conceptualization, Methodology, Software, Validation, Formal analysis, Data curation, Writing - original draft, Writing - review & editing, Visualization, Investigation. **Ricardo Mantilla:** Conceptualization, Methodology, Resources, Writing - review & editing, Supervision, Funding acquisition. **Witold F. Krajewski:** Conceptualization, Resources, Writing - review & editing, Supervision, Project administration, Funding acquisition. **Michael H. Cosh:** Writing - review & editing, Data curation.

Declaration of Competing Interest

None.

Acknowledgements

This study is funded by NASA SUSMAP (Science Utilization of the Soil Moisture Active-Passive Mission) program with Grant No. “15-0104” and Iowa Flood Center at The University of Iowa. First author would like to thank Radoslaw Goska at Iowa Flood Center for helping with data preparation. USDA is an equal opportunity provider and employer. Authors gratefully acknowledge the comments and suggestions of anonymous reviewers.

References

Babaeian, Ebrahim, Sadeghi, Morteza, Jones, Scott B., Montzka, Carsten, Vereecken, Harry, Tuller, Markus, 2019. Ground, proximal and satellite remote sensing of soil moisture. Rev. Geophys. https://doi.org/10.1029/2018RG000618. pp. 2018RG000618.

Beven, K., Germann, P.F., 1982. Macropores and water flows in soils. ISSN 00431397.

Bhatia, Rajendra, Davis, Chandler, 2000. A better bound on the variance. Am. Math. Mon. 107 (4), 353–357. https://doi.org/10.2307/2589180. ISSN 00029890.

Boone, Richard D., Nadelhoffer, Knute J., Canary, Jana D., Kaye, Jason P., 1998. Roots exert a strong influence on the temperature sensitivity of soil respiration. Nature 396 (6711), 570–572. https://doi.org/10.1038/25119. ISSN 00280836.

Brocca, L., Tullo, T., Melone, F., Moramarco, T., Morbidelli, R., 2012. Catchment scale soil moisture spatial-temporal variability. J. Hydrol. 422-423, 63–75. https://doi.org/10.1016/j.jhydrol.2011.12.039. ISSN 00221694.

Brocca, L., Zucco, G., Mittelbach, H., Moramarco, T., Seneviratne, S.I., 2014. Absolute versus temporal anomaly and percent of saturation soil moisture spatial variability for six networks worldwide. Water Resour. Res. 50 (7), 5560–5576. https://doi.org/10.1002/2014WR015684. ISSN 00431397.

Brocca, Luca, Ciabatta, Luca, Massari, Christian, Camici, Stefania, Tarpanelli, Angelica, 2017. Soil moisture for hydrological applications: open questions and new

opportunities. Water 9 (2). https://doi.org/10.3390/w9020140. ISSN 2073-4441.
Campbell Scientific Inc., 2012. CS650 and CS655 Water Content Reflectometers Instruction Manual. pp. 56. URL:www.campbellsci.com.
Chan, Steven K., Bindlish, Rajat, O'Neill, Peggy E., Njoku, Eni, Jackson, Tom, Colliander, Andreas, Chen, Fan, Burgin, Mariko, Dunbar, Scott, Piepmeier, Jeffrey, Yueh, Simon, Entekhabi, Dara, Cosh, Michael H., Caldwell, Todd, Walker, Jeffrey, Wu, Xiaoling, Berg, Aaron, Rowlandson, Tracy, Pacheco, Anna, McNairn, Heather, Thibeault, Marc, Martinez-Fernandez, Jose, Gonzalez-Zamora, Angel, Seyfried, Mark, Bosch, David, Starks, Patrick, Goodrich, David, Prueger, John, Palecki, Michael, Small, Eric E., Zreda, Marek, Calvet, Jean Christophe, Crow, Wade T., Kerr, Yann, 2016. Assessment of the SMAP passive soil moisture product. IEEE Trans. Geosci. Remote Sens. 54 (8), 4994–5007. https://doi.org/10.1109/TGRS.2016.2561938. ISSN 01962892.
Chaney, Nathaniel W., Roundy, Joshua K., Herrera-Estrada, Julio E., Wood, Eric F., 2015. High-resolution modeling of the spatial heterogeneity of soil moisture: applications in network design. Water Resour. Res. 51 (1), 619–638. https://doi.org/10.1002/2013WR014964. ISSN 19447973.
Chaney, Nathaniel W., Wood, Eric F., McBratney, Alexander B., Hempel, Jonathan W., Nauman, Travis W., Brungard, Colby W., Odgers, Nathan P., 2016. POLARIS: a 30-meter probabilistic soil series map of the contiguous United States. Geoderma 274, 54–67. https://doi.org/10.1016/j.geoderma.2016.03.025. ISSN 00167061.
Chaubell, Julian, Yueh, S., Entekhabi, D., Peng, J., 2016. Resolution enhancement of SMAP radiometer data using the Backus Gilbert optimum interpolation technique. In: 2016 IEEE International Geoscience and Remote Sensing Symposium (IGARSS). IEEE, pp. 284–287. https://doi.org/10.1109/IGARSS.2016.7729065. ISBN 978-1-5090-3332-4.
Chen, Quan, Zeng, Jiangyuan, Cui, Chenyang, Li, Zhen, Chen, Kun Shan, Bai, Xiaojing, Jia, Xu., 2018. Soil moisture retrieval from SMAP: a validation and error analysis study using ground-based observations over the little Washita watershed. IEEE Trans. Geosci. Remote Sens. 56 (3), 1398–1408. https://doi.org/10.1109/TGRS.2017.2762462. ISSN 01962892.
Cho, Eunsang, Choi, Minha, 2014. Regional scale spatio-temporal variability of soil moisture and its relationship with meteorological factors over the Korean peninsula. J. Hydrol. 516, 317–329. https://doi.org/10.1016/j.jhydrol.2013.12.053. ISSN 00221694.
Choi, Minha, Jacobs, Jennifer M., 2007. Soil moisture variability of root zone profiles within SMEX02 remote sensing footprints. Adv. Water Resour. 30 (4), 883–896. https://doi.org/10.1016/j.advwatres.2006.07.007. ISSN 03091708.
Ciach, Grzegorz J., Krajewski, Witold F., 1999. On the estimation of radar rainfall error variance. Adv. Water Resour. 22 (6), 585–595. https://doi.org/10.1016/S0309-1708(98)00043-8. ISSN 03091708.
Cornelissen, Thomas, Diekkrüger, Bernd, Bogena, Heye R., 2014. Significance of scale and lower boundary condition in the 3D simulation of hydrological processes and soil moisture variability in a forested headwater catchment. J. Hydrol. 516, 140–153. https://doi.org/10.1016/j.jhydrol.2014.01.060. ISSN 00221694.
Dorigo, W.A., Wagner, W., Hohensinn, R., Hahn, S., Paulik, C., Xaver, A., Gruber, A., Drusch, M., Mecklenburg, S., van Oevelen, P., Robock, A., Jackson, T., 2011. The International Soil Moisture Network: a data hosting facility for global in situ soil moisture measurements. Hydrol. Earth Syst. Sci. 15 (5), 1675–1698. https://doi.org/10.5194/hess-15-1675-2011. ISSN 1607-7938.
Entekhabi, Dara, Rodriguez-Iturbe, Ignacio, Castelli, Fabio, 1996. Mutual interaction of soil moisture state and atmospheric processes. J. Hydrol. 184 (1-2), 3–17. https://doi.org/10.1016/0022-1694(95)02965-6. ISSN 00221694.
Entekhabi, Dara, Njoku, Eni G., O'Neill, Peggy E., Kellogg, Kent H., Crow, Wade T., Edelstein, Wendy N., Entin, Jared K., Goodman, Shawn D., Jackson, Thomas J., Johnson, Joel, Kimball, John, Piepmeier, Jeffrey R., Koster, Randal D., Martin, Neil, McDonald, Kyle C., Moghaddam, Mahta, Moran, Susan, Reichle, Rolf, Shi, J.C., Spencer, Michael W., Thurman, Samuel W., Tsang, Leung, Zyl, Jakob Van, 2010. The soil moisture active passive (SMAP) mission. Proc. IEEE 98 (5), 704–716. https://doi.org/10.1109/JPROC.2010.2043918. ISSN 00189219.
Famiglietti, J.S., Devereaux, J.A., Laymon, C.A., Tsegaye, T., Houser, P.R., Jackson, T.J., Graham, S.T., Rodell, M., van Oevelen, P.J., 1999. Ground-based investigation of soil moisture variability within remote sensing footprints During the Southern Great Plains 1997 (SGP97) Hydrology Experiment. Water Resour. Res. 35 (6), 1839–1851. https://doi.org/10.1029/1999WR900047. ISSN 00431397.
Famiglietti, J.S., Rudnicki, J.W., Rodell, M., 1998. Variability in surface moisture content along a hillslope transect: Rattlesnake Hill, Texas. J. Hydrol. 210 (1–4), 259–281. https://doi.org/10.1016/S0022-1694(98)00187-5. ISSN 00221694.
Famiglietti, James S., Ryu, Dongryeol, Berg, Aaron A., Rodell, Matthew, Jackson, Thomas J., 2008. Field observations of soil moisture variability across scales. Water Resour. Res. 44 (1). https://doi.org/10.1029/2006WR005804. ISSN 00431397.
García, Gonzalo Martínez, Pachepsky, Yakov A., Vereecken, Harry, 2014. Effect of soil hydraulic properties on the relationship between the spatial mean and variability of soil moisture. J. Hydrol. 516, 154–160. https://doi.org/10.1016/J.JHYDROL.2014.01.069. ISSN 0022-1694.
Gebler, S., Hendricks Franssen, H.-J., Kollet, S.J., Qu, W., Vereecken, H., 2017. High resolution modelling of soil moisture patterns with TerrSysMP: a comparison with sensor network data. J. Hydrol. 547, 309–331. https://doi.org/10.1016/J.JHYDROL.2017.01.048. ISSN 0022-1694.
Grillakis, M.G., Koutroulis, A.G., Komma, J., Tsanis, I.K., Wagner, W., Blöschl, G., 2016. Initial soil moisture effects on flash flood generation – a comparison between basins of contrasting hydro-climatic conditions. J. Hydrol. 541, 206–217. https://doi.org/10.1016/j.jhydrol.2016.03.007. ISSN 00221694.
Guo, Li, Lin, Henry, 2018. Addressing Two Bottlenecks to Advance the Understanding of Preferential Flow in Soils, 1st ed. Elsevier Inc.https://doi.org/10.1016/bs.agron.2017.10.002. vol. 147, ISBN 9780128152836.
Hardie, Marcus, Lisson, Shaun, Doyle, Richard, Cotching, William, 2013. Determining the frequency, depth and velocity of preferential flow by high frequency soil moisture monitoring. J. Contam. Hydrol. 144 (1), 66–77. https://doi.org/10.1016/j.jconhyd.2012.10.008. ISSN 18736009.
Harrison, D.L., Scovell, R.W., Kitchen, M., 2009. High-resolution precipitation estimates for hydrological uses. Proc. Inst. Civil Eng. 162 (2), 125–135. https://doi.org/10.1680/wama.2009.162.2.125. ISSN 1741-7589.
Huffman, George J., Bolvin, David T., Braithwaite, Dan, Hsu, Kuo, Joyce, Robert, Kidd, Christopher, Nelkin, Eric J., Xie, Pingping, 2015. NASA Global Precipitation Measurement (GPM) Integrated Multi-satellitE Retrievals for GPM (IMERG). Algorithm Theoretical Basis Document (ATBD) Version 4.5, 26.
Kerr, Yann H., 2007. Soil moisture from space: where are we? Hydrogeol. J. 15 (1), 117–120. https://doi.org/10.1007/s10040-006-0095-3. ISSN 14312174.
Kim, Seungbum, 2013. Ancillary Data Report: Landcover Classification. (SMAP Science Document no. 042).
Koster, Randal D., Dirmeyer, Paul A., Guo, Zhichang, Bonan, Gordon, Chan, Edmond, Cox, Peter, Gordon, C.T., Kanae, Shinjiro, Kowalczyk, Eva, Lawrence, David, Liu, Ping, Lu, Cheng Hsuan, Malyshev, Sergey, McAvaney, Bryant, Mitchell, Ken, Mocko, David, Oki, Taikan, Oleson, Keith, Pitman, Andrew, Sud, Y.C., Taylor, Christopher M., Verseghy, Diana, Vasic, Ratko, Xue, Yongkang, Yamada, Tomohito, 2004. Regions of strong coupling between soil moisture and precipitation. Science 305 (5687), 1138–1140. https://doi.org/10.1126/science.1100217. ISSN 00368075.
Neelam, Maheshwari, Mohanty, Binayak P., 2015. Global sensitivity analysis of the radiative transfer model. Water Resour. Res. 51 (4), 2428–2443. https://doi.org/10.1002/2014WR016534. ISSN 19447973.
Njoku, Eni G., Entekhabi, Dara, 1996. Passive microwave remote sensing of soil moisture. J. Hydrol. 184 (1-2), 101–129. https://doi.org/10.1016/0022-1694(95)02970-2. ISSN 00221694.
Orchard, Valerie A., Cook, F.J., 1983. Relationship between soil respiration and soil moisture. Soil Biol. Biochem. 15 (4), 447–453. https://doi.org/10.1016/0038-0717(83)90010-X. ISSN 00380717.
Peel, M.C., Finlayson, B.L., McMahon, T.A., 2007. Updated world map of the Köppen-Geiger climate classification. Hydrol. Earth Syst. Sci. 11 (5), 1633–1644. https://doi.org/10.5194/hess-11-1633-2007. ISSN 16077938.
Qu, W., Bogena, H.R., Huisman, J.A., Vanderborght, J., Schuh, M., Priesack, E., Vereecken, H., 2015. Predicting subgrid variability of soil water content from basic soil information. Geophys. Res. Lett. 42 (3), 789–796. https://doi.org/10.1002/2014GL062496. ISSN 00948276.
Romano, Nunzio, 2014. Soil moisture at local scale: measurements and simulations. J. Hydrol. 516, 6–20. https://doi.org/10.1016/J.JHYDROL.2014.01.026. ISSN 0022-1694.
Rondinelli, Wesley J., Hornbuckle, Brian K., Patton, Jason C., Cosh, Michael H., Walker, Victoria A., Carr, Benjamin D., Logsdon, Sally D., 2015. Different rates of soil drying after rainfall are observed by the SMOS satellite and the south fork in situ soil moisture network. J. Hydrometeorol. 16 (2), 889–903. https://doi.org/10.1175/JHM-D-14-0137.1. ISSN 1525-755X.
Rosenbaum, U., Bogena, H.R., Herbst, M., Huisman, J.A., Peterson, T.J., Weuthen, A., Western, A.W., Vereecken, H., 2012. Seasonal and event dynamics of spatial soil moisture patterns at the small catchment scale. Water Resour. Res. 48 (10). https://doi.org/10.1029/2011WR011518. ISSN 00431397.
Ryu, Dongryeol, Famiglietti, James S., 2005. Characterization of footprint-scale surface soil moisture variability using Gaussian and beta distribution functions during the Southern Great Plains 1997 (SGP97) hydrology experiment. Water Resour. Res. 41 (12). https://doi.org/10.1029/2004WR003835. ISSN 00431397.
Shellito, Peter J., Small, Eric E., Colliander, Andreas, Bindlish, Rajat, Cosh, Michael H., Berg, Aaron A., Bosch, David D., Caldwell, Todd G., Goodrich, David C., McNairn, Heather, Prueger, John H., Starks, Patrick J., Velde, Rogier van der, Walker, Jeffrey P., 2016. SMAP soil moisture drying more rapid than observed in situ following rainfall events. Geophys. Res. Lett. 43 (15), 8068–8075. https://doi.org/10.1002/2016GL069946. ISSN 19448007.
Sivapalan, M., Beven, Keith, Wood, Eric F., 1987. On hydrologic similarity: 2. A scaled model of storm runoff production. Water Resour. Res. 23 (12), 2266–2278. https://doi.org/10.1029/WR023i012p02266. ISSN 19447973.
Stevens, 2018. Soil Sensor ®Users Manual.
Teuling, Adriaan J., Troch, Peter A., Mar 2005. Improved understanding of soil moisture variability dynamics. Geophys. Res. Lett. 32 (5), 1–4. https://doi.org/10.1029/2004GL021935. ISSN 00948276.
Topp, G.C., Davis, J.L., Annan, A.P., 1980. Electromagnetic determination of soil water content: measurements in coaxial transmission lines. Water Resour. Res. 16 (3), 574–582. https://doi.org/10.1029/WR016i003p00574. ISSN 19447973.
Wang, Tiejun, Franz, Trenton E., Zlotnik, Vitaly A., You, Jinsheng, Shulski, Martha D., 2015. Investigating soil controls on soil moisture spatial variability: Numerical simulations and field observations. J. Hydrol. 524, 576–586. https://doi.org/10.1016/j.jhydrol.2015.03.019. ISSN 00221694.
Western, Andrew W., Blöschl, Günter, 1999. On the spatial scaling of soil moisture. J. Hydrol. 217 (3–4), 203–224. https://doi.org/10.1016/S0022-1694(98)00232-7. ISSN 00221694.

Western, Andrew W., Zhou, Sen-Lin, Grayson, Rodger B., McMahon, Thomas A., Blöschl, Günter, Wilson, David J., 2004. Spatial correlation of soil moisture in small catchments and its relationship to dominant spatial hydrological processes. J. Hydrol. 286 (1-4), 113–134. https://doi.org/10.1016/j.jhydrol.2003.09.014. ISSN 00221694.

Yang, Kai, Wang, Chenghai, Bao, Hongyan, 2016. Contribution of soil moisture variability to summer precipitation in the Northern Hemisphere. J. Geophys. Res. 121 (20). https://doi.org/10.1002/2016JD025644. 12,108–12,124. ISSN 2169897X.

Yang, Yang, Dou, Yanxing, Liu, Dong, An, Shaoshan, 2017. Spatial pattern and heterogeneity of soil moisture along a transect in a small catchment on the Loess Plateau. J. Hydrol. 550, 466–477. https://doi.org/10.1016/j.jhydrol.2017.05.026. ISSN 00221694.

Zarlenga, A., Fiori, A., Russo, D., 2018. Spatial variability of soil moisture and the scale issue: a geostatistical approach. Water Resour. Res. 54 (3), 1765–1780. https://doi.org/10.1002/2017WR021304. ISSN 0043-1397.

Zhang, Jian, Howard, Kenneth, Langston, Carrie, Kaney, Brian, Qi, Youcun, Tang, Lin, Grams, Heather, Wang, Yadong, Cockcks, Stephen, Martinaitis, Steven, Arthur, Ami, Cooper, Karen, Brogden, Jeff, Kitzmillller, David, 2016. Multi-Radar Multi-Sensor (MRMS) quantitative precipitation estimation: Initial operating capabilities. Bull. Am. Meteorol. Soc. 97 (4), 621–638. https://doi.org/10.1175/BAMS-D-14-00174.1. ISSN 00030007.